Proton-Coupled Electron Transfer from Electrodes to Myoglobin in Ordered Biomembrane-like Films

Alaa-Eldin F. Nassar,[†] Zhe Zhang, Naifei Hu,[‡] and James F. Rusling*

Department of Chemistry, Box U-60, University of Connecticut, Storrs, Connecticut 06269-4060

Thomas F. Kumosinski

Eastern Regional Research Center, U.S. Department of Agriculture, Philadelphia, Pennsylvania 19118

Received: September 20, 1996; In Final Form: December 3, 1996[⊗]

Voltammetry and visible and infrared spectroscopy were used to explore protonation equilibria coupled to electron transfer between electrodes and the heme protein myoglobin (Mb) in thin liquid crystal films of didodecyldimethylammonium bromide (DDAB) and phosphatidylcholines (PC). Mb conformation and heme iron ligation in the films were controlled by the pH of the external solution. Acid−base equilibrium models successfully explained pH dependencies of Soret band absorbances, formal potentials, electron transfer rate constants, and electroactive surface concentrations of Mb in the films. A pK_{a1} of 4.6 in the Mb−lipid films is associated with protonation of histidine residues in hydrophobic regions of the Mb structure, possibly involving the proximal histidine bound to iron and/or the distal histidine in the heme pocket. At pH < 4.6, a partly unfolded *molten globule* form of Mb predominates in the films and is reduced directly. Native metmyoglobin [MbFe(III)−H_2O] appears to be the major species in films between pH 5.5 and 8. In this pH range, protonation of MbFe(III)−H_2O occurs prior to electron transfer, and a protonated form which may be a kinetic conformer accepts the electron. MbFe(III)−OH is formed in the films at pH > 9, and its one-electron reduction is also coupled to protonation.

Introduction

Conformational changes of proteins are possible rate-controlling steps in biological electron transfer.[1] Differences in conformation for different redox states have been established for cytochrome *c*[2] and other proteins.[3] Electrolysis of proteins has been combined with spectroscopy[4−7] to investigate redox-linked changes in secondary structure. FT-IR[5] and NMR[6] yielded detailed information on secondary structure for different protein redox states. FT-IR and visible spectroelectrochemistry of myoglobin (Mb) and hemoglobin in solution revealed structural differences between Fe(III) and Fe(II) forms for the polypeptide backbone and the hemes.[5b] Visible Soret band spectra can uncover changes in the heme environment, while FT-IR spectral band shapes can be used to monitor changes in protein conformation.[8]

Films providing biomembrane-like microenvironments are useful for the study of protein redox chemistry, as well as for applications in biosensors and catalysis. We recently reported stable, ordered, liquid crystal surfactant films in which direct electron transfer between electrodes and Mb was achieved.[9−12] Electron transfer rates for Mb in these films were up to 1000-fold larger than for the protein in solution on bare Au, Pt, and carbon electrodes. Spectroelectrochemistry showed that MbFe(III) was converted quantitatively to MbFe(II) in the absence of oxygen.[13] ESR anisotropy, polarized reflectance FT-IR, linear dichroism, and thermal phase transition studies showed that both Mb and surfactants are specifically oriented in these films. The surfactants are arranged in bilayers similar to lipid membranes.[9,11,12] Mb heme orientation was relatively independent of surfactant type and head group charge (i.e., +1, 0, −1), suggesting that Mb is at least partly imbedded in the surfactant bilayers.

We also used Mb−surfactant films for catalytic reductive dehalogenation of a series of organohalide pollutants.[13] The reductions mimic one type of action of the membrane-bound iron heme enzyme cytochrome P450.[14] Both oxidative and reductive biocatalysis with cytochrome P450 have as their initial step the transfer of an electron from a reductase enzyme to cytochrome P450. For catalytic reductions, this first electron transfer occurs under anaerobic conditions. Catalytic oxidations require oxygen.[15]

Mb can be made to catalyze oxidations[15−18] and reductions,[13,19,20a] similar to cytochrome P450. While clear differences in reactivities and specificities exist between the two proteins, Mb−surfactant films provide readily available models with which details of processes similar to important metabolic events can be investigated.

In this paper, the influence of pH on electrochemistry and protein conformation monitored by electronic and FT-IR absorption spectra is examined for Mb−surfactant films. Films of Mb and dialkylphosphatidylcholines or didodecyldimethylammonium bromide (DDAB) were used because they form lamellar liquid crystal phases with chemically reversible Mb voltammetry.[9−12] Results suggest that electron transfer to native MbFe(III)−H_2O in thin films of surfactants is coupled to protonation at pH > 5 and may involve a kinetic conformational intermediate at pH 5−8. At pH < 4.6, protonation of native MbFe(III)−H_2O in the films yields a stable, partly unfolded conformer which appears to be the main electron acceptor.

Experimental Section

Materials and Solutions. Horse myoglobin (Sigma) dissolved in buffer was passed through Amicon YM30 filters

[†]Present address: Battelle Institute, 2012 Tollgate Rd., Bel Air, MD 21015.

[‡]Permanent address: Chemistry Department, Beijing Normal University, Beijing, China.

[⊗] Abstract published in *Advance ACS Abstracts,* March 1, 1997.

S1089-5647(96)02896-9 CCC: $14.00

(30 000 MW cutoff).[10a] Concentrations after filtration were estimated by visible spectroscopy.[9] Dimyristoyl (DMPC) and dilauroyl (DLPC) phosphatidylcholines (99%) were from Sigma, and didodecyldimethylammonium bromide (DDAB, 99+%) was from Kodak. Dimethyl(ferrocenylmethyl)hexadecylammonium bromide (Fc-C16) and dimethyl(ferrocenylmethyl)dodecylammonium bromide (Fc-C12) were synthesized and purified as described previously.[20b] All other chemicals were reagent grade.

Buffers for voltammetry all contained 100 mM NaBr. Buffers were 25 mM citrate for pH 3.2−6, 25 mM phosphate for pH 7−8 and pH 11, and 25 mM borate for pH 9−10. Water was purified with a Barnstead Nanopure system to specific resistance >15 MΩ cm. Universal buffers of 10 mM each citric acid, sodium dihydrogen phosphate, and boric acid were used to prepare films for FT-IR spectroscopy, to maintain a relatively consistent spectral background.

Apparatus and Procedures. Methods and apparatus for cyclic voltammetry (CV) and square wave voltammetry (SWV) were described previously.[9−11] Oxygen was removed by purging solutions with purified nitrogen. Films were cast onto basal plane pyrolytic graphite (PG) disks (HPG-99, Union Carbide; geometric $A = 0.16$ cm^2) previously abraded on 600-grit SiC paper. Potentials are referred to the saturated calomel reference electrode (SCE). Cell resistance was about 100 Ω. Electronic compensation was used for CV such that ohmic drop of the cell was <2 mV. All experiments were done at 25 °C.

Films were cast onto PG electrodes from clear vesicle dispersions[12] of 0.5 mM DDAB or 2.5 mM phosphatidylcholines (PC) containing 0.065 mM Mb. Ten microliters of dispersion was spread evenly onto each electrode and dried overnight in air. Similar procedures were used to prepare films of DDAB or PC incorporating ferrocene amphiphiles Fc-C12 and Fc-C16.

Apparent heterogeneous electron transfer rate constants (k_s) were obtained by nonlinear regression analysis of SWV data. This procedure was previously shown to successfully fit data for myoglobin−surfactant films.[11b,20c] The model combines theory for SWV of a surface-confined species on an electrode[21] with a dispersion of p $E^{\circ\prime}$ values. The SWV current (i) is given by

$$i = \sum_{j=1}^{p} i_j \tag{1}$$

where i_j is the contribution of the jth of p classes of redox centers with formal potential $E^{\circ\prime}{}_j$ to the total current, given by

$$i_j = (nFA\Gamma_j^*)\frac{\Psi_j}{t_p} \tag{2}$$

Here, n is the number of electrons transferred per redox center, A is electrode area (cm^2), Γ_j^* is the total surface concentration (mol cm^{-2}) of the jth class, and t_p is the pulse width. Ψ_j is the dimensionless current:

$$\Psi_j = [(\kappa_{f,j} + \kappa_{b,j})\Gamma'_{0,j} - \kappa_{b,j}] \exp[-(\kappa_{f,j} + \kappa_{b,j})] \tag{3}$$

and

$$\Gamma''_{0,j} = \frac{\Psi_j + \kappa_{b,j}}{(\kappa_{f,j} + \kappa_{b,j})} \tag{4}$$

where $\Gamma'_{0,j}$ is the jth surface concentration ratio $\Gamma_{0,j}/\Gamma_j^*$ at time $t = 0$, $\Gamma''_{0,j}$ is the ratio $\Gamma_{0,j}/\Gamma_j^*$ at $t = t_p$, $\kappa_{f,j} = k_{f,j}t_p$, and $\kappa_{b,j} = k_{b,j}t_p$. Rate constants k_f and k_b are for forward and reverse electron transfer defined as in the Butler−Volmer equation,[22] given by

$$k_{f,j} = k_s t_p \exp[-\alpha(nF/RT)(E - E_j^{\circ\prime})] \tag{5}$$

and

$$k_{b,j} = k_s t_p \exp[(1 - \alpha)(nF/RT)(E - E_j^{\circ\prime})] \tag{6}$$

where k_s is the standard surface rate constant in s^{-1}, α is the electrochemical transfer coefficient, E is applied potential, $E_j^{\circ\prime}$ is the standard potential of jth class of redox centers, R is the gas constant, T is temperature in Kelvins, and F is Faraday's constant. Parameters used in the fitting procedure were the p $E_j^{\circ\prime}$ values, α, the average k_s, and either the p Γ_j^* or the total surface concentration.

Preliminary studies showed that the $E^{\circ\prime}$ dispersion model with $p = 5$ gave a reasonable compromise between acceptable goodness of fit, consistency of parameters, and time of computation. Each value of k_s and $E^{\circ\prime}$ reported is the average of analysis of six or more SWVs from which background had been subtracted. An alternative kinetic dispersion model with p k_s and p Γ_j^* parameters did not fit SWV data.

All nonlinear regression analyses were done with a program based on the Marquardt−Levenberg algorithm, assuming absolute errors in dependent variables.[23a] Goodness of fit was assessed by comparing standard deviation of the regression as well as computed and experimental data and their residuals. Parameter correlation matrices indicated that there were no significant correlations between parameters in any of the regression analyses, and fits beginning from different parameter starting points always gave the same final parameters within ±0.2%, indicating that the estimated parameters were unique sets in all cases. The best fit between models with different numbers of parameters, e.g. different p values in the SWV model, was chosen with the aid of the extra-sum-of-squares F-test,[23a] which considers the different numbers of degrees of freedom in the two models.

Films for spectroscopic analyses were cast from Mb−surfactant dispersions similar to those used to coat electrodes. Quartz was the substrate for UV−vis spectroscopy, and aluminum-coated glass was used for reflectance−absorbance FT-IR. Procedures were described in detail previously.[9,12]

Results

Influence of pH on Voltammetry of Myoglobin. The nearly reversible cyclic voltammograms (CV) of myoglobin (Mb) in insoluble surfactant films reflect exchange of electrons between the electrode and the heme Fe(III)/Fe(II) redox couple.[9−11] CVs showed a strong dependence on pH in films of DDAB or phosphatidylcholines (PC). The nearly reversible Mb heme Fe(III)/Fe(II) peaks in Figure 1 shifted negative and changed shape slightly with increasing pH for both types of surfactant. In general, changes with pH were reversible, and CVs similar to those in Figure 1 were obtained upon transferring a film from a buffer at a different pH.[23b]

CVs of Mb−surfactant films had symmetric peak shapes, and equal reduction and oxidation peak heights which were linear functions of scan rate from 0.002−2 V s^{-1}. These results are characteristic of thin layer electrochemical behavior,[24a] in which all electroactive MbFe(III) in the films is converted to MbFe(II) on the forward CV scan. Negative deviations from linearity occurred at >2 V s^{-1}, suggesting the onset of control by electrode kinetics and/or diffusion.

Films made with PCs became thinner after soaking in buffer for about 1 h, but then remained stable.[11b] The final thickness of Mb−PC films has been estimated at 0.5−1 μm by scanning electron microscopy. Films made with DDAB were stable as

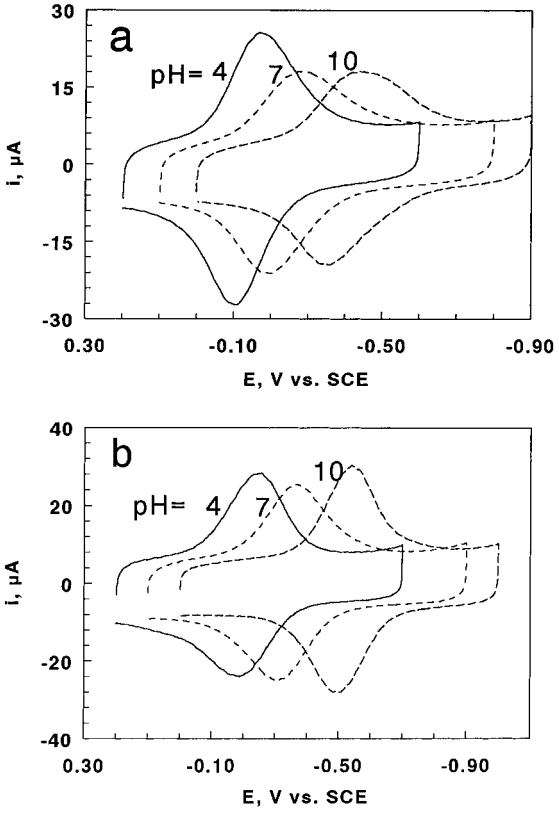

Figure 1. Cyclic voltammograms at 2 V s^{-1} in buffers containing 100 mM NaBr of (a) Mb−DDAB film on PG electrode and (b) Mb−DLPC film on PG electrode.

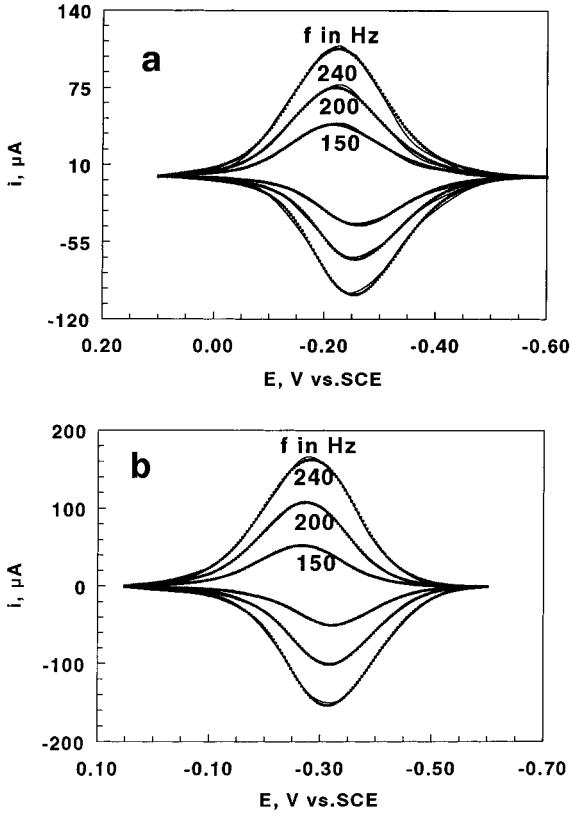

Figure 2. Forward and reverse square wave voltammograms for Mb−surfactant films on PG electrodes at 75 mV pulse height, 4 mV step height, and different frequencies (*f*), with background subtracted. Points are experimental data, and lines are best fits by nonlinear regression onto the model in eqs 1−6 using 5 $E_j^{\circ\prime}$ and 5 Γ_j^*(a) Mb−DDAB in pH 7.0 buffer, with best fits for average $k_s = 48 \pm 2$ s^{-1}, $\alpha = 0.48 \pm 0.01$, and $E^{\circ}_{avg}{}' = -0.241 \pm 0.001$ V vs. SCE; (b) Mb−DMPC in pH 6.0 buffer, with best fits for average $k_s = 63 \pm 8$ s^{-1}, $\alpha = 0.50 \pm 0.01$, and $E^{\circ}_{avg}{}' = -0.288 \pm 0.004$ V vs. SCE.

prepared and had similar thickness. The difference in this respect is due to the slight water solubility of the PCs used.[24b]

Square wave voltammetry (SWV) was used for quantitative kinetic analysis of the electrode reactions because of advantages in signal-to-noise and resolution over CV.[24c] When a model for SWV of a single species confined to an electrode surface[21] was fit onto experimental SWVs for Mb−surfactant films, forward and reverse current vs potential peaks were much broader than the theoretical shapes predicted by the model. Thus, we combined dispersion of $E^{\circ\prime}$ values[11b] with the above SWV theory to fit the data (see the Experimental Section).

Regression parameters were the p $E_j^{\circ\prime}$ values, α, the average k_s, and either the p Γ_j^*s or the total Mb surface concentration. Either of the latter choices of parameters gave similar results for p $E_j^{\circ\prime}$ values, α, and average k_s, but total surface concentration was somewhat overestimated from high-frequency SWVs compared to the more reliable CV integration. However, studies with noisy theoretical data computed using eqs 1−6 showed that relative distributions of Γ_j^*s were obtained accurately. Better quality fits and more consistent parameter values from scan to scan were obtained by analyzing the forward and reverse SWV curves simultaneously, rather than by analyzing the net current, which contained more noise.

Examples of analysis of SWV data for Mb−surfactant films demonstrate goodness of fit of the model over a range of frequencies (Figure 2). Results of regression analyses using individual Γ_j^* in the model were used to plot distribution diagrams as relative amounts of electroactive protein with each of the different $E_j^{\circ\prime}$ values. Roughly Gaussian distributions were obtained for all films (Figure 3) independent of the pH, although absolute heights and actual $E_j^{\circ\prime}$ values varied with pH. Average formal potentials and k_s values obtained from these analyses are discussed below.

Formal potentials ($E^{\circ\prime}$) of the Mb heme Fe(III)/Fe(II) couple in the films were obtained as midpoints between CV anodic

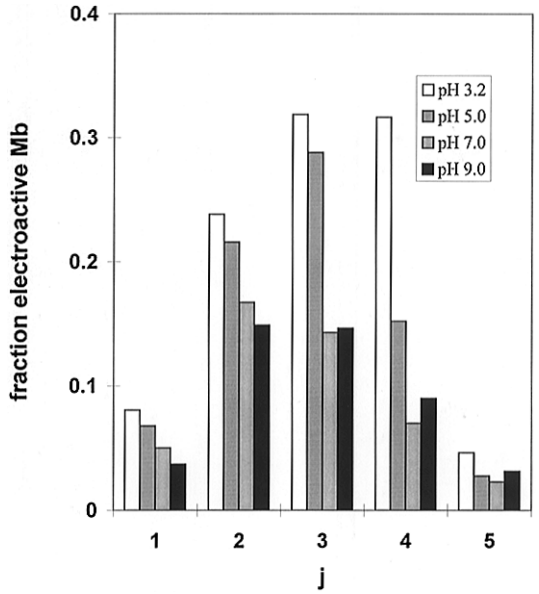

Figure 3. Distribution of relative fraction of electroactive Mb in Mb−DDAB films expressed as surface concentrations vs j for different $E_j^{\circ\prime}$ values resulting from analysis of SWV data with model in eqs having 5 $E^{\circ\prime}$s and their associated Γ_j^*. SWV pulse height 75 mV, frequency 200 Hz, step height 4 mV.

and cathodic peak potentials and also as the average of the $E_j^{\circ\prime}$ values from analyses of several SWV at each pH. The two methods gave good agreement. Plots of $E^{\circ\prime}$ vs pH for all films had linear regions from pH 5 up to about 11 (Figure 4). Average slopes in this pH range were between 51 and 56 mV/pH unit,

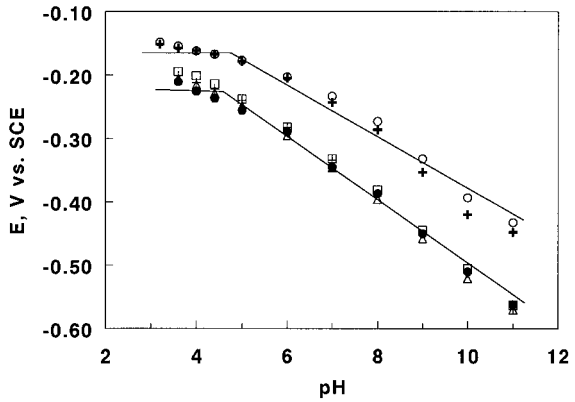

Figure 4. Influence of pH on formal potential for films of Mb−DDAB from CV (○) and SWV (+), Mb−DMPC from CV (□) and SWV (●), and Mb−DLPC from CV (+) and SWV (△). CV values are averages for scan rates from 0.1 to 2 V s^{-1}, SWV values are averages from fitting data at 60 and 75 mV pulse heights and frequencies between 100 and 240 Hz. Solid lines are representative of a coupled protonation (eq 7) with pK_{a1}'s of 4.9 for Mb−DDAB, and 4.6 for Mb−PC films.

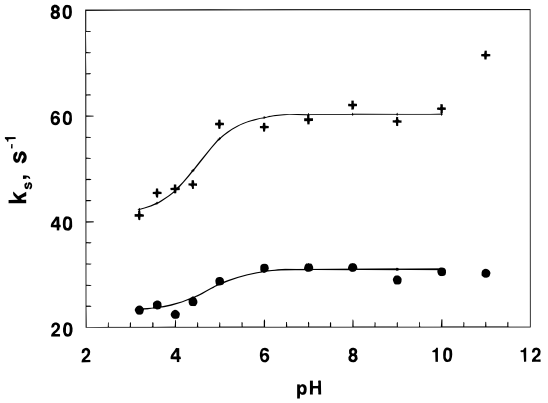

Figure 5. Influence of pH on heterogeneous rate constant k_s obtained as an average from analysis of SWV data at 60 and 75 mV pulse heights and frequencies between 100 and 240 Hz for Mb−DDAB film (●) with best fit from pH 3 to 10 (—) to eq 8 with pK_{a1} = 4.8 and m = 1, and for Mb−DMPC film (+) with best fit from pH 3 to 10 (—) to eq 8 with pK_{a1} = 4.5 and m = 1.

close to the 59 mV/pH expected at 25 °C for the transfer of one proton and one electron in a reversible reduction.[25] $E^{\circ\prime}$'s in PC films were about 100 mV more negative than in DDAB films, suggesting a specific influence of film environment which has been noted previously.[11b]

$E^{\circ\prime}$ values of both types of films were roughly independent of pH between pH 3.6 and 4.5 (Figure 4), although they shifted slightly positive at pH < 3.8. These pH dependencies resemble that for the electrochemical reduction of a weak acid,[25] in which the pH-dependent region is caused by participation of a proton in the electrode reaction. The intersection points at pH 4.7 ± 0.3 suggest that this protonation reaction of the protein has a pK_{a1} of about 4.7.

Average heterogeneous electron transfer rate constants (k_s) obtained from SWV increased with a sigmoid shape as pH was increased from the low pH range (Figure 5). Integrations of symmetric thin-layer CVs provided the surface concentration[24a] of electroactive protein. A sigmoid-shaped decrease in surface concentration was found for all Mb films as pH was increased in the low pH range (Figure 6), suggesting that external pH influences the fraction of electroactive protein.

Voltammetry of Ferrocene Amphiphiles in Surfactant Films. Films of the insoluble surfactants incorporating electroactive amphiphiles dimethyl(ferrocenylmethyl)hexadecylammonium bromide (Fc-C16) and dimethyl(ferrocenylmethyl)-dodecylammonium bromide (Fc-C12) were studied for comparison with the Mb−surfactant films. The one-electron oxidation of Fc-C12 and Fc-C16 occurs on the ferrocene moiety,[20b] and CV characteristics should not depend on pH.

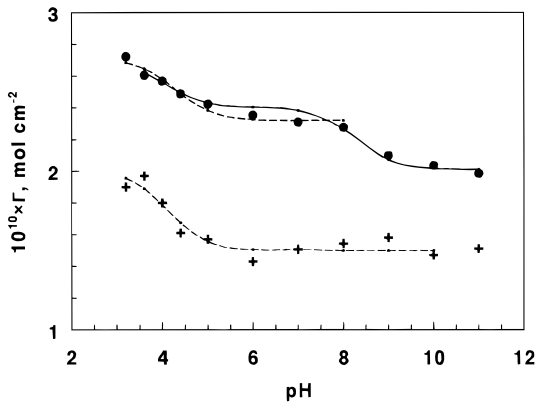

Figure 6. Influence of pH on average surface concentration (Γ) of electroactive Mb obtained from integration of reduction peaks of CVs at scan rates ≤ 0.1 V s^{-1} for Mb−DDAB film (●) with best fit from pH 3 to 8 (- - -) to eq 8 with pK_{a1} = 4.3 and m = 1, and best fit to eq 10 (—) with pK_{a1} = 4.1, m = 1, and pK_{a2} = 8.3, and for Mb−DLPC film (+) with best fit from pH 3 to 10 (- - -) to eq 8 with pK_{a1} = 4.1 and m = 1.

Films of the ferrocene amphiphiles were much less stable than those of Mb, but we were able to obtain CVs over the full pH range. No obvious trends in voltammetry of Fc-C12 or Fc-C16 were found with changing pH. Formal potentials did not vary with pH. For example, in a series of buffers from pH 3.2 to 11, Fc-C16 in DDAB films had an average $E^{\circ\prime}$ of 0.541 ± 0.005 V vs SCE, while Fc-C12 in DMPC films had an average $E^{\circ\prime}$ of 0.518 ± 0.003 V. These results imply that the pH dependence of Mb voltammetry does not result from the properties of the surfactants alone.

FT-IR Spectra of Mb in Films. Shapes of the amide infrared bands[8a,26] are sensitive to conformational changes in the polypeptide backbone of Mb. The amide I band (1700−1600 cm^{-1}) is caused by C═O stretching of peptide linkages. The amide II band (1600−1500 cm^{-1}) is a combination of N−H bending and C−N stretching. Amide bands of proteins consist of many overlapped components,[8] and resolution enhancement of the spectra is needed to identify conformational differences.[26] For this purpose, we used second-derivative FT-IR spectra,[2d,27a] as well as Fourier deconvoluted spectra.[26]

As reported previously,[9] reflectance−absorbance infrared (RAIR) spectra of Mb−surfactant films showed no large differences from films of Mb alone between pH 5.5 and 7.5, where the protein has its native conformation in solution. However, at pH ≤ 5.5, significant, reversible changes began to occur in the amide band shapes. Similar changes in spectra with pH were found at source incidence angles of 45°, 60°, and 75°.

Similar changes in amide I bands with pH were found for Mb in PC and DDAB films. To illustrate, we compare spectra in the second-derivative format[2d,27a] (Figure 7), which gave essentially the same results as a Fourier deconvolution−regression method.[26] The second derivative of a symmetric positive peak has a negative peak at the position of the original maximum, in between two smaller positive maxima. Thus, the strong negative peak at about 1659 cm^{-1} in spectra of the pure Mb films without surfactant at pH 5−7 (Figure 7a) is characteristic of a major component of the amide I band. This 1659 cm^{-1} band has been assigned to the α-helix.[8,26,27a] At pH 4, this peak[27b] becomes smaller and is accompanied by a new band close to 1631 cm^{-1}. This band has been assigned to extended features of the polypeptide backbone.[26,27a]

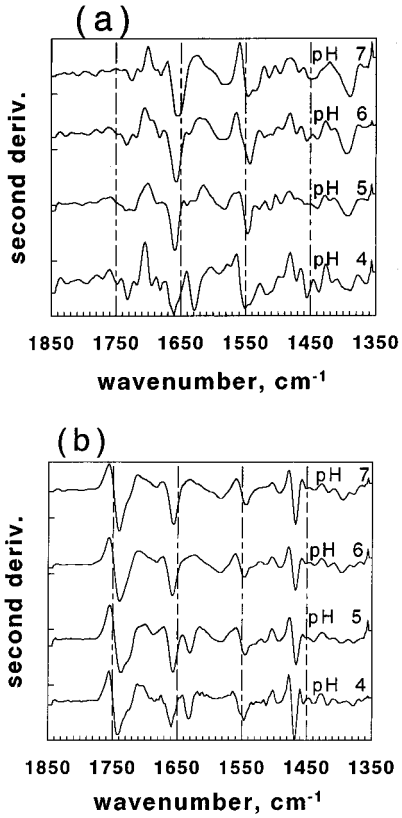

Figure 7. Second-derivative RAIR spectra at source incidence angle 60° of films prepared using buffers from pH 4 to 7: (a) Mb film; (b) Mb−DMPC film.

Second-derivative FT-IR spectra of Mb-PC films at pH 6 and 7 are similar to those of Mb alone at pH 5−7 in the amide I region. Differences in other frequency ranges include the PC ester carbonyl stretching band at 1742 cm^{-1}, weak broad absorbance features associated with PC and the universal buffer between about 1500 and 1550 cm^{-1}, and the CH_2 bending band of PC alkyl chains at 1465−1468 cm^{-1}. The amide I region of the second-derivative spectra at 1620−1700 cm^{-1} is not affected by these interferences (Figure 7b).

As pH decreased from 7 to 4, the band for Mb−PC films at 1657−1659 cm^{-1} decreases[27b] and is accompanied by a new band at slightly lower frequency. The new 1631 cm^{-1} peak is clearly evident at pH 5 and is stronger at pH 4 (Figure 7b). This new band assigned to extended protein backbone features[26,27] suggests unfolding of helices compared to the native-like Mb structure at pH 6 and 7. Second-derivative spectra for Mb−DDAB at pH 4 also showed a band at 1630 cm^{-1}, but not at pH 7.5, confirming increased extended chain features as pH decreased. Analysis of RAIR data by Fourier deconvolution−regression[26] suggested the loss of roughly 20% helix in the films when going from pH 7.5 to 4.

Visible Absorbance Spectra. The Soret band caused by visible absorbance by the Fe(III)heme in Mb is sensitive to pH.[28,29] Mb Soret bands in films and in buffers showed large decreases in absorbance below pH 5 and above pH 7.5. Between pH 6 and 9, the Mb−DDAB λ_{max} is about 415 nm, at slightly longer wavelengths than in Mb films or in solutions. At pH 4 the Mb−DDAB band shifted to 403 nm. The region between pH 4 and 3 also featured a sharp blue shift for Mb solutions.

Mb−PC films with adequate stability and absorbance could not be prepared on glass or quartz. However, Mb in bilayer vesicle dispersions of DMPC and DLPC showed similar changes in Soret bands with pH, with small differences from solution spectra.

Models for the Influence of pH. Equilibrium models were tested to describe the pH dependencies of spectroscopic and electrochemical parameters of Mb. Expressions of the form of $Y_{obs} = F(Y_k, [H^+], K_j)$ were constructed using the overall equilibrium approach,[23a] where the K_j are proton association constants and the Y_k are parameters characteristic of contributions of individual forms of the protein. Equation 7 explains all the data in the low-pH range (e.g. pH 3.2−8):

$$\mathrm{MbFe(III)} + m\mathrm{H}^+ \rightleftharpoons \mathrm{MbFe(III)H}_m \qquad K_1 \qquad (7)$$

where charges on the Mb species are omitted. Equation 7 represents the known multiple protonations of Mb as it is titrated with acid.[28−35]

If k_s and $\Gamma^*_{MbFe(III)}$ in the low-pH region are influenced by acid−base equilibria as in eq 7 prior to electron transfer, the mathematical formulation of this equilibrium should explain the k_s and $\Gamma^*_{MbFe(III)}$ vs pH data quantitatively. Thus, eq 8, based on eq 7,[23a] was used to fit data for pH dependencies of k_s and $\Gamma^*_{MbFe(III)}$ (Figures 5 and 6).

$$Y_{obs} = \frac{Y_0}{1 + K_1^m[H^+]^m} + \frac{Y_1 K_1^m[H^+]^m}{1 + K_1^m[H^+]^m} \qquad (8)$$

where Y_{obs} is the measured k_s or $\Gamma^*_{MbFe(III)}$, and Y_0 and Y_1 are parameters characteristic of that measured quantity for MbFe(III) and MbFe(III)H_m. Equation 8 was fit onto Y_{obs} vs pH data between pH 3.2 and 9 by nonlinear regression using Y_0, Y_1, and K_1 as parameters. Best fits were found for $m = 1$. Graphical examples illustrate goodness of fit (Figures 5 and 6).

While eq 8 also provided good fits of the Soret absorbance in the acidic pH region, the equilibrium[28a,b,29a] in eq 9 also needed to be considered to fit data over the entire pH range.

$$\mathrm{MbFe(III)-OH} + \mathrm{H}^+ \rightleftharpoons \mathrm{MbFe(III)-H_2O} \qquad K_2 \quad (9)$$

The mathematical expression embodying eqs 7 and 9 together[23a] is

$$Y_{obs} = \frac{Y_0}{1 + K_1^m[H^+]^m} + \frac{Y_1 K_1^m[H^+]^m}{1 + K_1^m[H^+]^m} + \frac{(Y_2 - Y_1)K_2[H^+]}{1 + K_2[H^+]} \qquad (10)$$

Equation 10 gave good fits onto spectroscopic Soret absorbance vs pH data by nonlinear regression using Y_0, Y_1, Y_2, K_1, and K_2 as parameters. Equation 10 also successfully fit $\Gamma^*_{MbFe(III)}$ data for Mb−DDAB over the full pH range (Figure 6a).

For ease of comparison, association constants found by regression analyses were converted to acid dissociation constants by using $pK_{aj} = -pK_j$. Values of pK_{a1} (Table 1) did not show significant variability in the different films and averaged 4.6. This is in good agreement with pK_{a1} for Mb in solution (Table 1) and with values reported previously in similar solutions.[28,29] Similar pK_{a1} values were found from electrochemical data on 20 μm thick Mb−DDAB films, as compared to the ca. 1 μm films discussed here. Values of pK_{a2} were similar in films, PC vesicles, and solution and were also comparable to those reported previously.[28a,b,29a]

Discussion

Dependence of Spectra and Voltammetry on pH. Previous studies by ESR, absorption spectroscopy, and linear dichroism showed[9,12] that myoglobin in DDAB and PC films is in the high-spin MbFe(III)−H_2O form at solution pH between 5.5 and 7.5. This native state features a proximal histidine bound to iron

TABLE 1: Equilibrium Constants[a] for Mb From Regression Analysis of Measured Quantity vs pH Data

sample	measured quantity	model	pK_{a1}	pK_{a2}
Mb−DDAB films	k_s (s^{-1})	eq 8	4.8[c]	
	Γ^* (mol cm^{-2})	eq 8	4.3[c]	
	Γ^* (mol cm^{-2})	eq 10	4.1[c]	8.3[c]
	$E^{o\prime}$	eq 8	4.9 ± 0.2	
	Soret band absorbance	eqs 8 & 10	4.2 ± 0.8	8.4 ± 0.7[d]
Mb soln., $I = 55$ mM[b]	soret band absorbance	eqs 8 & 10	4.1 ± 0.5	8.3 ± 0.5
Mb soln., $I = 105$ mM[b]	soret band absorbance	eqs 8 & 10	4.4 ± 0.2	8.8 ± 0.2
Mb−DLPC films	k_s (s^{-1})	eq 8	4.6[c]	
	Γ^* (mol cm^{-2})	eq 8	4.1[c]	
	$E^{o\prime}$	eq 8	4.7 ± 0.2	
Mb−DMPC films	k_s (s^{-1})	eq 8	4.5[c]	
	Γ^* (mol cm^{-2})	eq 8	4.0[c]	
	$E^{o\prime}$	eq 8	4.6 ± 0.2	
Mb in DMPC vesicles	soret band absorbance	eqs 8 & 10	4.7 ± 0.1	8.8 ± 0.1[e]

[a] Expressed as acid dissociation constants, see text. pK_a given with standard errors from the regression analyses. All for $m = 1$ unless otherwise noted. [b] I = ionic strength. [c] Errors are within ±0.5. [d] $m = 2$. [e] $m = 5$.

below the plane of the heme and a distal histidine hydrogen-bonded to ligated water above the heme.[31,34,35]

Reversible changes in electrochemical and spectroscopic features with pH show that Mb properties within the films are controlled by the acidity of the solution in which the films reside. The pH-independent voltammetry found for ferrocene amphiphiles in DDAB and PC films supports the view that pH-dependent voltammetry of Mb−surfactant films is characteristic of Mb and does not reflect properties of the surfactants.

Visible and FT-IR spectra confirmed native MbFe(III)−H_2O as the major Mb species present in the films between pH 5.5 and 8. At pH < 5, the UV−vis spectra suggest partial protein denaturation in the films, as observed previously in aqueous solutions.[28,29] The spectral changes in films at pH > 8 are attributed to dissociation of the axial water of MbFe(III)−H_2O (eq 9), a known solution equilibrium.[28a,b,29a]

FT-IR spectra (Figure 7) suggest partial unfolding of the Mb secondary structure at pH < 5.5. They show that at pH 5.5−7.5, as reported previously,[9,12] Mb in the films has a secondary structure similar to the native state, with about 75% helix.[26] Partial unfolding of the protein involving loss of helices is found at pH 4 in surfactant-free films (Figure 7a). Unfolding is clearly indicated in DDAB and PC films at pH 4 by the second derivative peak at 1630 cm^{-1} (Figure 7b). A smaller amount of unfolding is found at pH up to 5.5. The band at 1659 cm^{-1} is associated with α-helices, and its intensity is lost at the expense of the 1630−1631 cm^{-1} band assigned to extended polypeptide. Roughly 20% helix is lost from pH 7.5 to 4. The surfactant films facilitate partial unfolding at pH values slightly larger than the transition between native and partly unfolded intermediates in the absence of surfactant.

The model in eqs 7 and 8 provides good fits (Table 1 and Figures 4−6) for the pH dependencies of all electrochemical data for Mb−surfactant films between pH 3.2 and 8, and in some cases up to pH 10. For Mb−DDAB films, eq 10 fits the $\Gamma^*_{MbFe(III)}$ vs pH data as well and gave reasonable pK_{a1} and pK_{a2} values (Table 1). Other plots of k_s or $\Gamma^*_{MbFe(III)}$ vs pH showed changes at pH > 9, reflecting the onset of the additional equilibrium. However, data were insufficient in the higher pH region to obtain good values of pK_{a2}, since films became less stable at pH > 11. On the other hand, eq 10 gave good fits onto Soret absorbance data, and pK_{a1} and pK_{a2} values were obtained (Table 1).

Agreement of pK_{a1} values in DDAB and PC films and in solution suggests that similar effects are operative on the iron heme and on Mb secondary structure in the films and in solution. Visible spectra in films are characterized by a blue shift and decreased absorbance of the Soret band as pH decreases below pK_{a1}, as found for Mb in solution.[28a,b,29a]

Among numerous probes of solution equilibria of Mb,[28−35] NMR is probably the most structurally revealing. NMR has been used to provide pK_a values for protonation of individual amino acid side chains of horse and sperm whale myoglobin.[31,34,35] The distal and proximal histidines of Mb were found to have pK_{a1} values between pH 4.3 and 5, as do four other histidines in hydrophobic regions of the native protein.[34] The iron-bound proximal histidine and/or the distal histidine in the heme pocket are likely to be associated with the pK_{a1} for Mb in the films. The bond between the proximal histidine and Fe(III) may be broken below pH 5.[29c,34]

A comment on proton stoichiometry is also in order. The overall equilibrium models in eqs 8 and 10 will give $m = 1$ for the titrations of multiple sites with very similar pK_a values.[23a] The value $m = 1$ associated with pK_{a1} from analyses of electrochemical data (Table 1) is understandable because electron transfer is most likely to be sensitive mainly to protonation of a histidine in the vicinity of the electroactive iron. Soret band data in aqueous solutions also gave $m = 1$, and the histidines titrated have similar pK_a's consistent with NMR results.[34,35] The $m = 2$ found for the Soret band data in DDAB films suggests that film spectra begin to differentiate the histidine pK_{a1} values. The $m = 5$ from Soret band data for Mb in the PC vesicle solution suggests differentiation of most of the individual histidines titrated in the acidic pH range.

Average pK_{a2} values for dissociation of the water bound to the Fe(III)heme of Mb (Table 1) were very similar in solution, DDAB films, and PC vesicles. Values are similar to those reported previously in water.[28a,b,29a]

Reduction Pathways of Mb in the Films. Spectral identifications of the main Mb species residing in the films in different pH ranges can be used as the starting point for molecular interpretations of the electrochemical reaction pathways. In buffer solutions between pH 5.5 and 8, native high-spin MbFe(III)−H_2O predominates. At pH > 9, low-spin MbFe(III)−OH is the major species present.

At pH between about 3.5 and 5, spectroscopic studies of myoglobin and apomyoglobin in solution have identified a stable, partly unfolded intermediate[28−35] known as a *molten globule*. While much of this work concentrated on apomyoglobin, myoglobin is known to have a similar structure.[31,35] Compared to the native state, the molten globule intermediate has B, C, D, and E helices unfolded.[31] This involves about a 30% loss of helix on going from native to the intermediate structure. FT-IR observations of significant helix unfolding at pH 4 in the films (Figure 7) suggest that a *molten globule*-like myoglobin represents a major protein fraction at pH below 4.6.

Voltammetric characteristics for Mb in DDAB and PC films show similar dependencies on pH. Plots of $E^{o\prime}$ vs pH (Figure

SCHEME 1

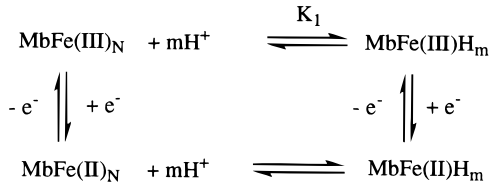

4) analyzed by using the theory of electrochemical reduction of weak acids[25] leads to similar conclusions and pK_{a1} values as analysis of k_s or $\Gamma^*_{MbFe(III)}$ vs pH data with the equivalent eq 8. That is, reduction of Mb between pH 5 and 11 in DDAB and PC films occurs by the transfer of one electron and one proton.

$\Gamma^*_{MbFe(III)}$ in the Mb films increases at low pH (Figure 6), and analysis gave an average pK_{a1} value of about 4.1. The increase in surface concentration of electroactive Mb in the films is the result of protonation of MbFe(III)$-H_2O$, increasing the fraction of electroactive Mb in the films, presumably via a conformational change to a *molten globule* conformer. This suggests that similar protonations with similar pK_{a1} values (Table 1) are associated with the pH dependence of $E^{\circ\prime}$ and k_s (Figures 4 and 5). Protonation occurs *prior* to the transfer of an electron. If the protonation occurred after the electron transfer, the amount of electroactive Mb, i.e. $\Gamma^*_{MbFe(III)}$, *would not increase* with pH at lower pH.

Electrochemical changes in the films at pH < 5 are well correlated with conformational changes in the protein found by spectroscopy. FT-IR and visible spectra suggest that some of the helices of the protein are unraveled in the films at low pH, as in solution.[28,29,31,34,35] These changes are correlated with the pH dependence of $\Gamma^*_{MbFe(III)}$, $E^{\circ\prime}$, and k_s suggesting that at pH < 4.6 the protonated, partly unfolded *molten globule* conformer of Mb becomes the main electron acceptor.

It is noteworthy that MbFe(II) was reported to show a decrease in the IR amide I α-helix bands near 1664 and 1654 cm^{-1} and an increase in intensity in the 1630−1640 cm^{-1} region with respect to native MbFe(III)$-H_2O$.[5b] Thus, the pathway for reduction of native MbFe(III)$-H_2O$ to MbFe(II) involves partial unfolding of protein helices.

Scheme 1 for reduction of native (N) MbFe(III)$_N$ at pH 5.5−8 in DDAB and PC films is consistent with our results. Theoretical analysis has shown[1] that electron transfer between proteins proceeds sequentially when coupled to conformational change. In Scheme 1, this suggests that protonation and attendant conformational rearrangement occur, followed by the electron transfer. A direct path from MbFe(III)$_N$ to MbFe(II)$_N$ is unlikely because it has a higher energy barrier than this sequential pathway.[1]

The top equation of Scheme 1 is similar to eq 7. Electron transfer occurs from the electrode to MbFe(III)H$_m$, consistent with the observed pH dependence of $\Gamma^*_{MbFe(III)}$, $E^{\circ\prime}$, and k_s. Electrochemical reduction is coupled to this equilibrium close to the electrode−film interface by removing MbFe(III)H$_m$, thus facilitating protonation of additional protein molecules in this interfacial region.

Comparisons of our pK_{a1} values with pK_a's of Mb side chains obtained by NMR[34,35] suggest that protonation of histidines controls the pH dependence of the electrochemical reaction.[36] Proximal and distal histidines are closest to the heme iron which accepts the electron, and their protonations are possible important factors. A recent study showed that conversion of the distal histidine of sperm whale myoglobin to hydrophobic or polar but non-hydrogen-bonding amino acids increased the reversibility of electron transfer from bare electrodes in solution due to alteration of the hydrogen-bonding network involving the axial water ligand on Fe(III).[37a] Protonation of the distal histidine may serve a similar function. Indeed, recent studies in our laboratory showed that electron transfer to partly unfolded (protonated) Mb in solution at pH 4.8 on bare basal plane PG electrodes was much more reversible than at pH > 5.5, at which voltammetric peaks could not be observed.[37b]

Direct reduction of the predominant species MbFe(III)$_N$ in the films at pH > 5 is inconsistent with the experimental results. In such a case, neither $\Gamma^*_{MbFe(III)}$ nor $E^{\circ\prime}$ of MbFe(III)$_N$ would depend on pH.[25] There is no direct evidence for conformational equilibrium involving MbFe(II), but we include this in Scheme 1 as a possibility.

It is difficult to assess how much of the full conformational change[5b] from MbFe(III)$_N$ to MbFe(II)$_N$ is associated with the proton-coupled electron transfer event between pH 5.5 and 8. We can estimate the time scale of unfolding processes from a study of the refolding of *molten globule* apomyoglobin (without heme) to the native apoprotein, which is first order with a decay time about 1 s.[38] Using this value, pK_{a1} in the films, and the principle of microscopic reversibility, we estimated that conversion of native to *molten globule* Mb would require about 15 s at pH 6, and longer at higher pH. Thus, full conversion from native to *molten globule* Mb would take too long to influence our SWV results, obtained on the millisecond time scale.

For the above reason, it is unlikely that the equilibrium *molten globule* Mb is the electron acceptor at pH > 5.5. This is consistent with the different k_s values at pH > 5.5 and pH < 4 (Figure 5), where *molten globule* Mb is reduced directly, implying electron transfer to a different species at pH > 5.5.

Nevertheless, kinetic intermediates of varying stability usually exist along protein-folding paths.[39] MbFe(III)$_N$ is unlikely to remain in the intact native conformation after protonation. We may speculate about the protonation driving fast conversion to a kinetic unfolding intermediate prior to electron transfer, which could then accept the electron, but definitive evidence supporting this point has yet to be obtained.

At pH < 4.6, the partly unfolded *equilibrium molten globule-like* MbFe(III) predominates in the films. The relative pH independence of $E^{\circ\prime}$ at pH < 4.6 suggests that this form is reduced directly. The slight positive drift in $E^{\circ\prime}$ as pH decreases to the smallest values used (Figure 4) probably reflects the onset of a more completely unfolded form of the protein.[31,32]

The pathway for electron transfer is less certain at pH > 9. Spectroscopic data show that the dissociation in eq 9 occurs in the films with an average pK_{a2} of 8.6 (Table 1). However, $E^{\circ\prime}$ continues to vary at pH > 9 with a slope indicating a single protonation coupled to electron transfer. No breaks in this pH range that would indicate a change in the nature of the species reduced can be discerned (Figure 4). Values of k_s do not change much in this pH range, except for a sharp increase in PC films at the highest pH values (Figure 5). $\Gamma^*_{MbFe(III)}$ is nearly constant in PC films, but decreases slightly in DDAB films at pH > 8 (Figure 6). For the latter films, analysis with eq 10 gave a pK_{a2} of 8.3, similar to that in solution (Table 1).[40] The results suggest reduction of a different species at pH > pK_{a2} than at lower pH. However, the pH dependence of $E^{\circ\prime}$ suggests that the predominant species, MbFe(III)$-$OH, at pH > 9 may not be reduced directly, but may be protonated prior to electron transfer. Although proton transfer could follow electron transfer, this would not be expected to influence $\Gamma^*_{MbFe(III)}$ in the DDAB films.

Conclusions

Results suggest that protonation precedes electron transfer from electrodes to aquometmyoglobin in films of DDAB and phosphatidylcholines in solutions of pH 5.5−8. A *molten globule* conformer accepts electrons directly at pH < 4.6. At

pH > 8 in these films, MbFe(III)−H_2O dissociates to MbFe(III)−OH. Its reduction is also accompanied by proton transfer.

In addition to demonstrating the effects of proton-coupled electron transfer from an electrode to a protein in a biomembrane-like environment, this work illustrates the usefulness of ordered surfactant films for detailed studies of protein redox chemistry. Recent extensions of these films have been made to other proteins and enzymes.[41]

Acknowledgment. This publication was supported by U. S. PHS Grant No. ES03154 from the National Institute of Environmental Health Sciences (NIEHS), NIH. Its contents are solely the responsibility of the authors and do not necessarily represent the official views of NIEHS, NIH. N.H. is grateful for financial support from the National Natural Science Foundation of China.

References and Notes

(1) Hoffman, B. M.; Ratner, M. A. *J. Am. Chem. Soc.* **1987**, *109*, 6237−6243, and references therein.

(2) For some recent studies, see: (a) Rosen, P.; Pecht, I. *Biochemistry* **1976**, *15*, 775−786. (b) Feng, Y.; Roder, H.; Englander, S. W. *Biochemistry* **1990**, *29*, 3494−3504. (c) Turner, D. T.; Williams, R. J. P. *Eur. J. Biochem.* **1993**, *211*, 555−562. (d) Dong, A.; Huang, P.; Caughey, W. S. *Biochemistry* **1992**, *31*, 182−189.

(3) For examples, see: (a) Blumenfeld, L. A.; Burbaev, D. S.; Davydov, R. M.; Kubrina, L. N.; Vanin, A. F.; Vilu, R. O. *Biochim. Biophys. Acta* **1975**, *379*, 512−516. (b) Ashby, G. A.; Thorneley, N. F. *Biochem. J.* **1987**, *246*, 455−465. (c) DiSpriito, A. A.; Balny, C.; Hooper, A. B. *Eur. J. Biochem.* **1987**, *162*, 299−304. (d) Miura, S.; Ichikawa, Y. *J. Biol. Chem.* **1991**, *266*, 6252−6258. (e) Brown, E. D.; Wood, J. M. *J. Biol. Chem.* **1993**, *268*, 8972−8979.

(4) (a) Simone, M. J.; Kreishman, G. P. *Anal. Biochem.* **1983**, *132*, 142−146. (b) Hildebrandt, P.; Stockburger, M. *Biochemistry* **1989**, *28*, 6710−6721.

(5) (a) Moss, D.; Nabedryk, E.; Breton, J.; Mantele, W. *Eur. J. Biochem.* **1990**, *187*, 565−572. (b) Schlereth, D. D.; Mantele, W. *Biochemistry* **1992**, *31*, 7494−7502. (c) Schlereth, D. D.; Fernandez, V. M.; Mantele, W. *Biochemistry* **1993**, *32*, 9199−9208.

(6) Battistuzzi, G.; Borsari, M.; Ferretti, S.; Sola, M.; Soliani, E. *Eur. J. Biochem.* **1995**, *232*, 206−213.

(7) (a) Yuan, X.; Sun, S.; Hawkridge, F. M.; Chlebowski, J. F.; Taniguchi, I. *J. Am. Chem. Soc.* **1990**, *112*, 5380−5381. (b) Nishiyama, K.; Hawkridge, F. M. *Biochem. Biophy. Res. Commun.* **1994**, *205*, 1724−1728.

(8) (a) Susi, H.; Byler, D. M. *Methods Enzymol.* **1986**, *130*, 290. (b) Krimm, S.; Bandekar, J. *Adv. Protein Chem.* **1986**, *38*, 183−363.

(9) Rusling, J. F.; Nassar, A.-E. F. *J. Am. Chem. Soc.* **1993**, *115*, 11891−11897.

(10) (a) Nassar, A.-E. F.; Willis, W. S.; Rusling, J. F. *Anal. Chem.* **1995**, *67*, 2386−2392. (b) Rusling, J. F.; Nassar, A-E. F. *Langmuir* **1994**, *10*, 2800−2806.

(11) (a) Nassar, A.-E. F.; Narikiyo, Y.; Sagara, T.; Nakashima, N.; Rusling, J. F. *J. Chem. Soc., Faraday Trans.* **1995**, *91*, 1775−1782. (b) Zhang, Z.; Rusling, J. F. *Biophys. Chem.*, in press.

(12) Nassar, A.-E. F.; Zhang, Z.; Chynwat, V.; Frank, H. A.; Rusling, J. F.; Suga, K. *J. Phys. Chem.* **1995**, *99*, 11013−11017.

(13) Nassar, A.-E. F.; Bobbitt, J. M.; Stuart, J. D.; Rusling, J. F. *J. Am. Chem. Soc.* **1995**, *117*, 10986−10993.

(14) (a) Castro, C. E.; Wade, R. S.; Belser, N. O. *Biochemistry* **1985**, *24*, 204−210. (b) Li, S.; Wackett, L. P. *Biochemistry* **1993**, *32*, 9355−9361.

(15) (a) Ortiz de Montellano, P. R., Ed. *Cytochrome P450*; Plenum: New York, 1986. (b) Schenkman, J. B., Greim, H., Eds. *Cytochrome P450*; Springer-Verlag, Berlin, 1993.

(16) Ortiz de Montellano, P. R.; Catalano, C. E. *J. Biol. Chem.* **1985**, *260*, 9265−9271.

(17) (a) Arduini, A.; Eddy, L.; Hochstein, P. *Arch. Biochem. Biophys* **1990**, *281*, 41−43. (b) Rao, S. I.; Wilks, A.; Hamberg, M.; Ortiz de Montellano, P. R. *J. Biol. Chem.* **1994**, *269*, 7210−7216.

(18) Kelman, D. J.; DeGray, J. A.; Mason, R. P. *J. Biol. Chem.* **1994**, *269*, 7458−7463.

(19) (a) Wade, R. S.; Castro, C. E. *J. Am. Chem. Soc.* **1973**, *95*, 231−234. (b) Bartnicki, E. W.; Belser, N. O.; Castro, C. E. *Biochemistry* **1978**, *17*, 5582−5586.

(20) (a) Hamachi, I.; Noda, S.; Kunitake, T. *J. Am. Chem. Soc.* **1991**, *113*, 9625−9630. (b) Peng, W.; Zhou, D.-L.; Rusling, J. F. *J. Phys. Chem.* **1995**, *99*, 6986−6993, and references therein. (c) Cell ohmic drop could result in small errors in k_s (<10%). These errors are independent of pH and are less than the relative standard deviation of k_s estimated from replicate SWVs (±20%). Errors resulting from ohmic drop in the other parameters are negligible.

(21) O'Dea, J. J.; Osteryoung, J. *Anal. Chem.* **1993**, *65*, 3090−3097.

(22) Bard, A. J.; Faulkner, L. R. *Electrochemical Methods*; Wiley: New York, 1980.

(23) (a) Rusling, J. F.; Kumosinski, T. F. *Nonlinear Computer Modeling of Chemical and Biochemical Data*; Academic Press: New York, 1996; pp. 87−116. (b) The exception to this occurred at the extreme pH values, where a small (<10%) decrease in current was observed when films were kept for 3−5 h in a buffer of pH 3.2 or 11, then transferred to a buffer of the other pH.

(24) (a) Murray, R. W. In *Electroanalytical Chemistry*; Bard, A. J., Ed.; Marcel Dekker: New York, 1984; Vol. 13, pp 191−368. (b) Cevc, G.; Marsh, D. *Phospholipid Bilayers*; Wiley: New York, 1987. (c) Osteryoung, J.; O'Dea, J. J. In *Electroanalytical Chemistry*; Bard, A. J., Ed.; Marcel Dekker: New York, 1986; Vol. 14, pp 209−308.

(25) (a) Meites, L. *Polarographic Techniques*, 2nd ed.; Wiley: New York, 1965; pp 282−284. (b) Bond, A. M. *Modern Polarographic Methods in Analytical Chemistry*; Marcel Dekker: New York, 1980; pp 29−30.

(26) (a) Kumosinski, T. F.; Unruh, J. J. In *Molecular Modeling*; Kumosinski, T. F., Leibman, M. N., Eds.; ACS Symposium Series 576; Washington, DC, 1993; pp 71−98. (b) Rusling, J. F.; Kumosinski, T. F. *Nonlinear Computer Modeling of Chemical and Biochemical Data*; Academic Press: New York, 1996; pp 117-134.

(27) (a) Dong, A.; Huang, P.; Caughey, W. S. *Biochemistry* **1990**, *29*, 3303−3308. (b) These peaks show small shifts with pH, appearing in Mb films at 1655 cm^{-1} at pH 7, 1657 cm^{-1} at pH 6, 1659 cm^{-1} at pH 5, and 1661 cm^{-1} at pH 4. In Mb−PC films, frequencies are 1657 cm^{-1} at pH 7, 1659 cm^{-1} at pH 6, 1657 cm^{-1} at pH 5, and 1659 cm^{-1} at pH 4. The low frequency band was consistently near 1631 cm^{-1} at pH 4 and 5.

(28) (a) Theorell, H.; Ehrenberg, A. *Acta Chem. Scand.* **1951**, *5*, 823−848. (b) George, P.; Hanania, G. *Biochem. J.* **1952**, *52*, 517−523. (c) Herskovits, T. T.; Jaillet, H. *Science* **1969**, *163*, 282−285.

(29) (a) Brunori, M.; Giacometti, G. M.; Antonini, E.; Wyman, J. *J. Mol. Biol.* **1972**, *63*, 139−152. (b) Takahashi-Ushijima, E.; Kihara, H. *Biochem. Biophys. Res. Commun.* **1982**, *105*, 965−968.

(30) (a) Puett, D. *J. Biol. Chem.* **1973**, *248*, 4623−4634. (b) Tang, H.-L.; Chance, B.; Mauk, A. G.; Powers, L. S.; Reddy, K. S.; Smith, M. *Biochem. Biophys. Acta* **1994**, *1206*, 90−96.

(31) Yang, A.-S.; Honig, B. *J. Mol. Biol.* **1994**, *237*, 602−614.

(32) (a) Goto, Y.; Fink, A. L. *J. Mol. Biol.* **1990**, *214*, 803−805. (b) Stigter, D.; Alonso, D. O. V.; Dill, K. A. *Proc. Natl. Acad. Sci. U.S.A.* **1991**, *88*, 4176−4180.

(33) Friend, S. H.; Gurd, F. R. N. *Biochemistry* **1979**, *18*, 4612−4619; 4620−4630.

(34) Bashford, D.; Case, D. A.; Dalvit, C.; Tennant, L.; Wright, P. E. *Biochemistry* **1993**, *32*, 8045−8056

(35) Cocco, M. J.; Kao, Y.-H.; Phillips, A. T.; Lecomte, J. T. J. *Biochemistry* **1992**, *31*, 6481−6491.

(36) Mb in a hydrogel membrane[36b] showed a complex pH dependence of $E^{o\prime}$ that was very different from that reported in Figure 2. The effect of pH in that study is probably related to interactions of Mb with the hydrogel. (b) Niu, J.; Guo, Y.; Dong, S. *J. Electroanal. Chem.* **1995**, *399*, 41−46.

(37) (a) Van Dyke, B. R.; Saltman, P.; Armstrong, F. A. *J. Am. Chem. Soc.* **1996**, *118*, 3490−3492. (b) Onuoha, A. C.; Rusling, J. F. Work in progress.

(38) Jennings, P. A.; Wright, P. E. *Science* **1993**, *262*, 890−895.

(39) Wolnyes, P. G.; Onuchi, J. N.; Thirumalai, D. *Science* **1995**, *267*, 1619−1620.

(40) (a) This difference in the DDAB and PC films may reflect a difference in internal pH. DDAB can preferentially attract OH^- to the vicinity of the cationic head groups.[40b] This may make the effective pH in DDAB films slightly higher than the effective pH in the phosphatidylcholine films having zwitterionic head groups, with no net charge. This might explain why the equilibrium in eq 9 is detected at a lower pH in the DDAB films. (b) Gounili, G.; Miaw, C. L.; Bobbitt, J. M.; Rusling, J. F. *J. Colloid Interface Sci.* **1992**, *153*, 446−456.

(41) (a) Bianco, P.; Haladjian, J. *J. Electroanal. Chem.* **1994**, *367*, 79−84. (b) Bianco, P.; Haladjian, J. *Electrochim. Acta* **1994**, *39*, 911−916. (c) Hanzlik, J.; Bianco, P.; Haladjian, J. *J. Electroanal. Chem.* **1995**, *380*, 287−290. (d) Bianco, P.; Haladjian, J. *Electroanalysis* **1995**, *7*, 442−446. (e) Tominaga, M.; Yanagimoto, J.; Nassar, A.-E. F.; Rusling, J. F.; Nakashima, N. *Chem. Lett.* **1996**, 523−524. (f) Lu, Z.; Huang, Q.; Rusling, J. F. *J. Electroanal. Chem.*, in press. (g) Huang, Q.; Lu, Z.; Rusling, J. F. *Langmuir* **1996**, *12*, 5472−5480.